Research Article Vol. 2, No. 1 / January 2015 / Optica 18

Optical Fourier synthesis of high-repetition-rate pulses

David S. Wu, David J. Richardson, and Radan Slavík*

Optoelectronics Research Centre, University of Southampton, Southampton, SO17 1BJ, UK

**Corresponding author: r.slavik@soton.ac.uk*

Received 22 September 2014; revised 18 November 2014; accepted 23 November 2014 (Doc. ID 223313); published 12 January 2015

The ultimate goal in the generation of optical signals is optical arbitrary waveform generation, which would allow the generation of wide-bandwidth optical signals with arbitrary amplitude and phase profiles (e.g., custom-shaped short optical pulses or advanced telecommunications signals). Here we investigate a new route toward this goal based upon the coherent combination of multiple signals generated at different wavelengths from different lasers. We show how to address the various challenges associated with this approach and demonstrate the generation of 100 GHz repetition rate waveforms by combining five semiconductor lasers phase locked, via injection locking, to a common optical frequency comb. Independent control of the optical power and phase of each laser enabled the generation of customized waveforms. Our technique be should readily scalable to a larger number of lasers, promising a flexible source of ultrastable, high-repetition rate, large-bandwidth (>1 THz), shot-noise-limited, high-power optical waveforms.

OCIS codes: (140.3520) Lasers, injection-locked; (320.5540) Pulse shaping; (070.0070) Fourier optics and signal processing.

http://dx.doi.org/10.1364/OPTICA.2.000018

1. INTRODUCTION

Optical arbitrary waveform generation is an actively pursued area of research as it could be used to generate customized signals with very high bandwidths. For example, it would be possible to generate waveforms with more than 1 THz bandwidth as opposed to the tens of gigahertz currently possible using electronics-based waveform generators. The ultimate goal is to achieve full dynamic optical arbitrary waveform generation that would be able to generate any continuous waveform of interest, e.g., for high-capacity data transmission in telecommunications [1,2].

In practice, it is more straightforward to realize so-called static arbitrary waveform generation, where repetitive pulse trains are generated. Although the speed at which the repetitive waveforms can be modified is limited, it still has numerous applications across a wide range of fields. Some selected examples include nonlinear signal processing [3,4], coherent control of molecular processes [5,6], spectroscopy [7], and optical communications [8]. Further examples can be found in the following review articles [9–11].

Static arbitrary waveform generation is commonly achieved by reshaping short pulses using optical filters to alter the spectral amplitude and phase profiles of an initial pulse to generate output pulses with the desired temporal profile and repetition rate. This commonly requires the initial pulse train to be spectrally dispersed to allow the different frequency components to be manipulated separately. It is common to spatially disperse the pulse, e.g., using gratings, and to alter the amplitude and phase of the different frequency components using a spatial light modulator, e.g., a liquid crystal on silicon (LCoS) modulator [12]. The filtered spectral components are then recombined to form the desired waveform. The update rate of the existing spatial light modulators is generally sufficient for static arbitrary waveform generation. However, when fast dynamic waveform generation is required, each spectral component needs to be modulated with an in-phase/quadrature-phase (I/Q) type modulator as described in detail in [1].

Spatial filtering of different frequency components allows for a wide range of different waveforms to be generated. The high popularity of this technique allowed it to be quickly

developed into a commercially available product. This technique, although very useful, suffers from several drawbacks. Despite high-resolution LCoS modulators now being available, each pixel has a limited damage threshold that limits the power that can be launched into the pulse shaper. Moreover, as this device is based on attenuating the unwanted part of the signal, it may suffer from low energetic efficiency, further reducing the optical power available at its output. Reamplification of the output degrades the signal-to-noise ratio (SNR), which may be detrimental for the targeted application, especially when high levels of amplification are needed, such as for nonlinear signal processing. Spectral filtering may also impose stringent requirements on the optical pulse source in terms of its stability. Furthermore, the repetition rate of the shaped pulses must be a multiple of the original repetition rate, and it must have large enough optical bandwidth. To summarize, the main limitations of this technique are (i) low energetic efficiency, (ii) limited SNR, and (iii) the dependence on the availability of a suitable optical pulse source.

Our work uses an alternative approach to generating arbitrarily shaped pulses and is based on direct synthesis of the desired signals rather than reshaping pregenerated pulses. Optical Fourier synthesis is the process of combining multiple continuous-wave lasers operating at different wavelengths to form pulse trains. The amplitude and phase profile of the pulse train can be customized by independently controlling the amplitude and phase of each laser as they are combined.

The advantage of directly synthesizing the pulse train is that the repetition rate can be readily changed by tuning the operating frequencies of the individual lasers. High energy efficiency can be achieved by using Fourier synthesis, as only the required frequency components are generated. A spectral disperser is also not required to separate the individual frequency components, although a multiplexer with sufficient resolution is still required to combine the lasers with minimal loss. In contrast to spectral filtering, which is an inherently lossy process, Fourier synthesis can directly generate high average power pulses by using high-power lasers. For example, by using 100 mW per laser, as available with commercial semiconductor DFB lasers, it should be possible to directly generate Watt level signals using 10 or so lasers without the requirement for any amplification. First, this allows the generation of high-power pulses, even at spectral regions where no high-power amplifiers exist. Second, the individual laser outputs are added coherently, while their noise is added incoherently, which improves the SNR of the output signal as compared with that of the individual lasers.

Optical Fourier synthesis would be practical only when many lasers can be integrated on the same chip. This is simply due to the practical challenges of utilizing many individual lasers (potentially tens or hundreds), which would result in a complicated, bulky, and expensive instrument. Fortunately, this is becoming possible today due to the advances made in the field of optical integration [13]. However, a simple integration and combination of lasers on a single chip would not be enough as coherent pulses can only be synthesized if the relative frequencies of the lasers are precise multiples of the desired pulse repetition rate and their phase relations are well controlled. In this article, we suggest and demonstrate how to address these challenges, paving the route to this new class of high-performance devices.

Low-repetition-rate (120 MHz) Fourier synthesis has already been demonstrated in the 1970 s [14] by phase locking up to five CO_2 lasers using heterodyne optical phase lock loops. High-repetition-rate Fourier synthesis up to 1.8 THz was later (1999–2001) demonstrated by Hyodo and co-workers [15–17] using three lasers. One of the lasers was phase locked to a frequency component generated by the other two lasers using nonlinear mixing such that the relative frequency between the three lasers was always equal. This technique, however, may be challenging to scale up to many lasers.

In this article, we address the challenges of optical Fourier synthesis using simple low-cost semiconductor lasers that could be integrated in a straightforward manner. In our prototype system, we generated stable 100 GHz pulses using five semiconductor lasers. Coherence between the lasers was achieved by phase locking them to an optical frequency comb. We generated pulses of various shapes by controlling the relative powers and phases of the individual laser outputs. The level of control we had of the phase properties was demonstrated by generating pulses that were precompensated for chromatic dispersion incurred during propagation through 2 km of optical fiber.

2. PHASE LOCKING TO AN OPTICAL FREQUENCY COMB

The optical frequency comb generator used in our demonstration of Fourier synthesis was an erbium-doped fiber mode-locked laser with a comb spacing of 250 MHz. This generated a wide spectrum of equally spaced comb modes that could be used as a frequency reference for Fourier synthesis. However, we expect that this could be replaced with a much simpler optical comb, such as those generated by modulating a continuous-wave laser [18]. It is worth mentioning that our technique does not put any strict constraints on the flatness of the comb spectrum. Semiconductor lasers (slave lasers) were phase locked to individual comb modes. Since the comb modes had an equal frequency spacing, the slave lasers were chosen to be locked to different comb modes such that the lasers themselves have an equal frequency spacing. For example, slave lasers locked 400 comb modes away from one another would have a frequency spacing of 100 GHz. The lasers became coherent with one another after they were phase locked to the common frequency comb, and hence they could be combined together coherently.

We phase locked our slave lasers using optical injection locking [19,20], where many comb modes were injected into the slave laser optical cavity simultaneously without prior isolation of individual comb modes, e.g., by using narrow-band filtering. Each comb mode injected into the slave laser could be considered as a separate continuous-wave master laser that the slave laser can lock to. Injection locking occurred when the frequency detuning between the slave laser and the comb mode was within the locking range. The size of the locking range was dependent on the injection ratio, defined as the power per

injected comb mode relative to the output power of the slave laser.

Low injection ratios (less than −50 dB) were used to limit the size of the locking range and prevent the slave laser from simultaneously locking to multiple comb modes, also strongly relaxing requirements on the comb source power. However, this made the slave laser susceptible to becoming unlocked due to frequency drifts, which caused the detuning to exceed the narrow locking range. This was overcome by using a simple electronic feedback loop to keep the detuning at a fixed value [21–24]. The bandwidth requirements of this feedback loop were modest due to the slow nature of the frequency drifts. In our previous work [24], a similar feedback loop was implemented (less than 30 Hz bandwidth), which allowed for long-term locking for over 8 h. The slave laser was found to have very low levels of frequency variation (Allan deviation: 9.7×10^{-17} at 1 s averaging time) and low phase noise (phase noise: 0.02 rad^2 integrated from 100 Hz to 500 MHz) relative to the comb mode it was locked to. The phase noise was minimized by using an optimal injection ratio and by suppressing the detuning-dependent amplification of residual comb modes injected into the slave laser [25].

The technique described above is scalable with comb spacing and could allow for wider spaced combs to be used (e.g., 10 GHz). This could result in improved energy efficiency, since fewer comb modes need to generated. Furthermore, the performance of the injection locking is expected to improve since it would allow for the use of larger injection ratios due to the reduced effects of the adjacent residual comb modes [25]. The widest possible comb spacing that can be used is ultimately limited by the bandwidth of the RF components required for the feedback loop to maintain a constant detuning between the slave laser and the comb mode it is locked to.

3. FOURIER SYNTHESIS SETUP

A. Slave Laser Ensemble

Five slave lasers were used for the demonstration of Fourier synthesis in this article. While this number is modest, our approach allows for a straightforward extension to a significantly larger number of lasers. The lasers used were all discrete mode semiconductor lasers [26] (Fabry–Perot-like lasers operating at a single wavelength) packaged into butterfly modules with no in-built isolator to allow for optical injection via the front facet. The output powers ranged from +2 to +12 dBm with a specified linewidth of less than 200 kHz. Each of the slave lasers utilized the feedback system from [24] to keep the detuning at a fixed value, which minimized the amplification of residual comb modes.

A schematic of how the slave lasers were set up is shown in Fig. 1. The optical frequency comb was demultiplexed into multiple channels separated by 100 GHz using an arrayed waveguide grating (AWG). Each of these channels had a 3 dB bandwidth of 50 GHz, containing approximately 200 comb modes. Different AWG channels were used for optical injection into different slave lasers. Each channel was connected to an optical variable attenuator (VOA) and polarization controller (PC) prior to the slave laser to control the injection ratio and to align the polarization of the slave signal to that of the laser output. The injection ratio for each laser was approximately −63 dB, which corresponded to the optimum value found in [24]. Optical injection was achieved by using a three-port circulator; however, a 2 × 2 coupler could be used instead for an integrated setup. Alternatively, the optical frequency comb could be injected via the rear facet [27]. Further, photonic integration would allow all the components to operate along one polarization axis (e.g., TE polarization), and thus the PCs used in our current fiber embodiment (in front of and behind each of the slave lasers) would not be needed.

10% of the output power of the slave laser was tapped off for the electronic feedback loop [24] to maintain the injection locking. The remaining 90% was connected to another VOA and PC, as well as a fiber stretcher based phase shifter (PS). This allowed control of the amplitude, polarization, and phase of the individual slave lasers as they are combined together using another AWG. The setup in Fig. 1 will be referred to as the slave laser ensemble for the remainder of this article. Polarization maintaining (PM) components and optical fiber could be used in this setup, which would eliminate the need for all the PCs.

The approximate operating wavelengths and the relative frequencies of the five locked slave lasers are given in Table 1. This combination of lasers will generate waveforms with a repetition rate of 100 GHz. The waveforms targeted in this article were based on a spectrum with a sinc-like profile as shown in Fig. 2. The components at ±200 GHz had amplitudes of zero, and hence lasers at those components were not required. This demonstrates one of the advantages of Fourier synthesis, in which only nonzero spectral components need to be generated, allowing for large bandwidths with a limited number of required lasers.

B. Phase Stabilization and Control

The generation of stable waveforms via Fourier synthesis required accurate and stable control of the relative phases between the slave lasers. Although each slave laser exhibited a high degree of phase stability from the phase locking process, they were susceptible to phase fluctuations relative to one

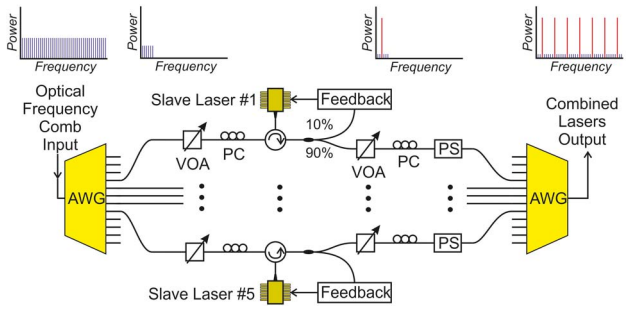

Fig. 1. Schematic of the slave laser ensemble, which contains and combines the injection locked lasers. AWG, arrayed waveguide grating; VOA, variable optical attenuator; PC, polarization controller; PS, fiber phase shifter. The optical spectrum is illustrated at the top of the figure for one of the AWG channels.

Table 1. Slave Laser Indexing

Laser Index	Wavelength (nm)	Relative Frequency (GHz)
#1	1548.8	+300
#2	1549.4	+100
#3	1550.2	0
#4	1551.0	−100
#5	1552.6	−300

another as they were multiplexed together by the AWG. This was due to thermally induced variations in the optical fiber (length of over 5 m in our setup) that connected each of the lasers to the AWG. This caused changes in the optical path length of each laser and hence changed their relative phases as they were combined. With the help of passive stabilization (fibers taped down, setup enclosed in a box), the relative phase between two of the slave lasers was found to drift by 2π over a period of approximately 30 min.

Active stabilization of these relative phases was implemented using the PSs in the slave laser ensemble as shown in Fig. 3. To generate error signals for controlling these PSs, various elegant solutions exist, e.g., digital phase lock loop techniques [28,29]. Such methods introduce dithers of different frequencies via the PSs, allowing for the extraction of multiple error signals using a single photodetector (PD). However, in our proof-of-principle experiment, this was achieved in a more cumbersome (but easier to implement) way by tapping off a portion of the output of the slave laser ensemble, which was first amplified using an erbium-doped fiber amplifier (EDFA), and frequency shifting it by 35 MHz by using an acousto-optic modulator (AOM). This was combined with the original frequency comb used for optical injection such that each slave laser would generate a 35 MHz beat signal with the original comb mode that it was locked to. The beat signals were separated from one another using an AWG and converted into electrical signals using PDs, as shown in Fig. 3.

The electrical beat signal from each laser was isolated using 50 MHz low-pass filters (LPFs) and was amplified using low-noise radio frequency (RF) amplifiers. One of these beat signals was used as a reference to measure the relative phase of the other beat signals using RF mixers and LPFs (3 kHz).

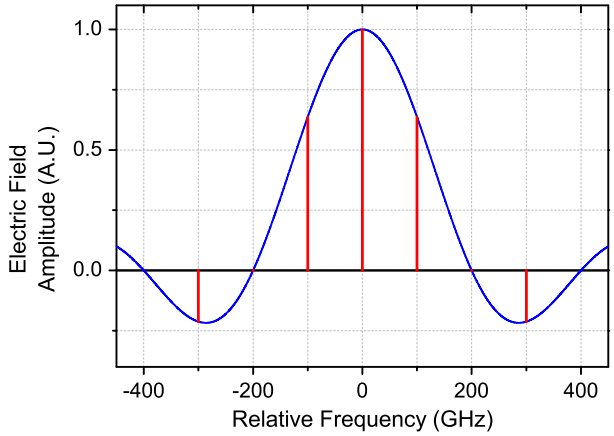

Fig. 2. Illustration of a sinc-shaped spectrum envelope (blue) realized with five discrete nonzero components (red).

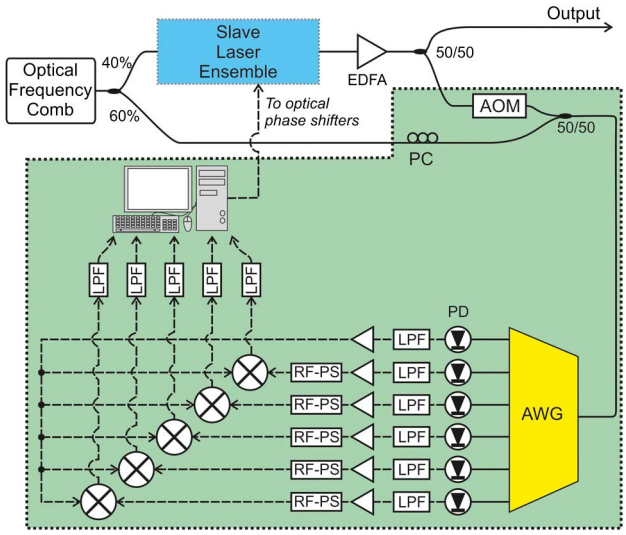

Fig. 3. Schematic of the phase stabilization setup. The 'slave laser ensemble' contains the setup shown in Fig. 1. EDFA, erbium-doped fiber amplifier; AOM, acousto-optic modulator; PD, photodetector; LPF, low-pass filter; RF-PS, radio frequency phase shifter.

The measured relative phase of the RF beat signals did not directly correspond with the relative optical phases between the slave lasers due to unmatched optical and RF path lengths. However, it allowed the relative optical phases to be stabilized by keeping the relative RF phase at a fixed value using a feedback loop. This corresponded to keeping the relative optical phase at a fixed, albeit unknown, value. The low bandwidth requirements for this feedback system allowed a personal computer (running LabView) to be used as the feedback controller with an approximate bandwidth of 10 Hz. The feedback acted on optical PSs, which were either piezoelectric (PZT) based or simple resistive heater based fiber stretchers.

The relative optical phases of the slave lasers were controlled by using RF phase shifters (RF-PSs) prior to mixing the RF beat signals. This was because a relative phase shift between the RF signals corresponded directly to a relative optical phase shift of the same amount.

It should be noted that dynamic arbitrary waveform generation via spectral slicing is conceivable by altering the slave laser ensemble in Fig. 1—in particular, by replacing the VOA and PS at the output of each slave laser with I/Q modulators, reducing the frequency spacing between the lasers to match the modulators' bandwidth, and modifying the phase stabilization technique described here (as it currently relies on measuring the relative phase between the CW slave laser and the comb mode it is locked to).

C. Waveform Measurement

The portion of the slave laser output not used for the phase stabilization was used to measure the generated waveforms as shown in Fig. 4. It was sent to a programmable optical filter (Finisar Waveshaper) to allow for the measurement of the relative phases of the slave lasers. The programmable filter on its own was capable of performing pulse shaping via spatial dispersion and filtering; however, it was only used here as a

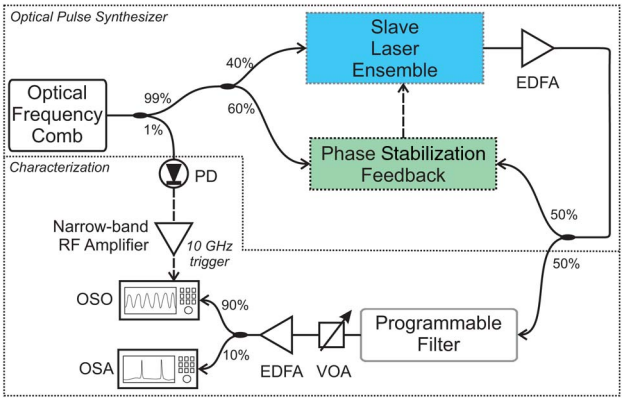

Fig. 4. Schematic of the full setup used for generating and measuring Fourier synthesized waveforms. The 'phase stabilization feedback' includes the components within the dotted box in Fig. 3. OSO, optical sampling oscilloscope; OSA, optical spectrum analyzer.

wavelength selective switch for calibration purposes. This will be discussed further in Section 4.

The high-repetition-rate waveforms targeted in this article required an optical sampling oscilloscope (OSO) to accurately measure their temporal power profiles. The OSO was triggered using an RF clock at 10 GHz, which was extracted from the optical frequency comb by measuring the 40th harmonic of the repetition rate. This was detected using a high-bandwidth PD, and the 10 GHz signal was isolated and amplified to the required power by using a narrow-band RF amplifier (10.0 ± 0.1 GHz). The OSO was specified to have a bandwidth of 500 GHz and an internal timing jitter of 100 fs. To overcome the limited sensitivity of the OSO, the output of the programmable filter was amplified using an EDFA. The optical spectrum was measured by tapping off a portion of the optical signal prior to the OSO and using an optical spectrum analyzer (OSA).

4. SYNTHESIZED WAVEFORMS

A. Calibration

Although the relative phases of the slave lasers were stabilized using the feedback described in the previous section, their actual values were unknown and needed to be measured and calibrated. Figure 5(a) shows the optical power profile of the waveform generated by the five slave lasers, with stabilized but random phases, measured on the OSO (9600 samples). The waveform repeats itself every 10 ps, which corresponded to a repetition rate of 100 GHz. The slave lasers were set to have equal powers as shown in the optical spectrum in Fig. 5(b). The spectrum shows that lasers #1 and #2 have small spectral peaks approximately 0.25 nm from the lasing wavelength. The origin of these were unclear but were inherent to the lasers since they were present even with no optical injection.

The relative phases were measured by using the programmable filter as a wavelength selective switch to isolate pairs of slave lasers by suppressing the others. An isolated pair of lasers generated a sinusoidal beat signal on the OSO. The phase of

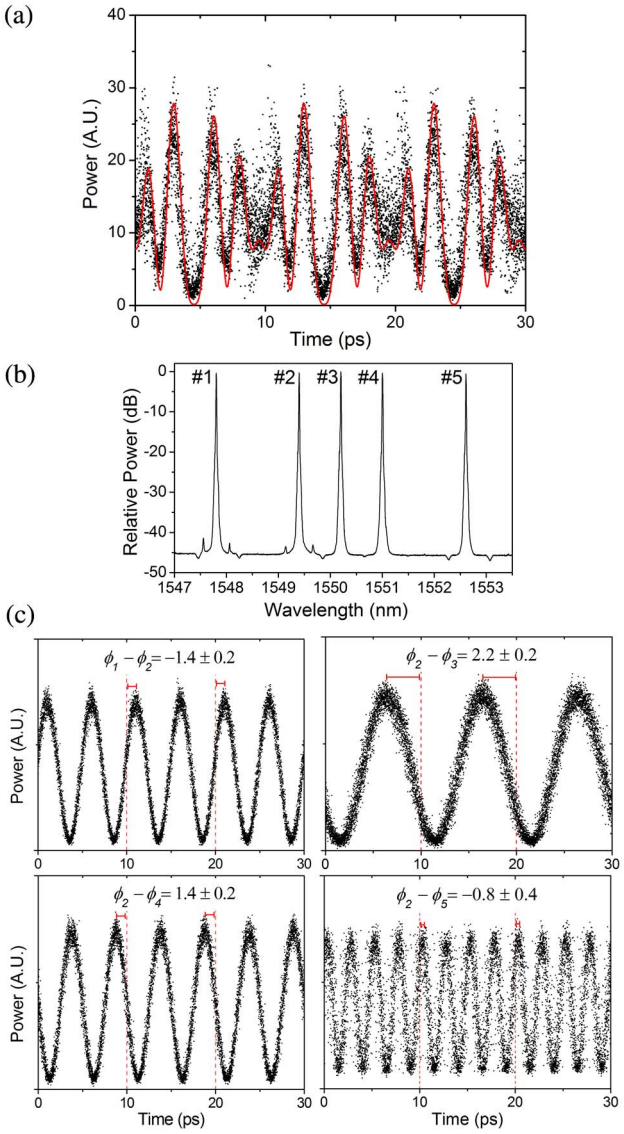

Fig. 5. (a) Temporal waveform of the uncalibrated slave lasers [dots, measured; red line, calculated using calibration data shown in (c)], and (b) corresponding spectrum. (c) Measured relative phases of the slave lasers with respect to laser #2.

this beat signal corresponded to the relative phase between the two lasers. Laser #2 was used as the reference laser, with the relative phases of the other lasers measured with respect to it.

The use of the programmable filter to generate these beat signals could be avoided by isolating pairs of slave lasers using the attenuators within the slave laser ensemble. However, the attenuators used in our setup were manually controlled, making the programmable filter far more convenient. Indeed, this could be overcome by using electrically controlled attenuators.

The measurements of the relative phases are shown in Fig. 5(c). Laser #5 was found to be noisier compared to the other slave lasers, as can be seen from the beat signal it generated with laser #2. This was due to its laser driver that was different from those used to drive the other lasers. The error associated with these measurements (given in Fig. 5) was calculated from the timing jitter in the measured beat signals due

to the OSO jitter, noise from the slave lasers, and noise from the injection locking process. The noise from the injection locking process is expected to be reduced by using a wider spaced frequency comb since the residual comb modes would introduce less noise [25]. The measured values for the relative phases and powers of the slave lasers were used to calculate an expected waveform. This was plotted against the measured waveform in Fig. 5(a) (red line), and there is good agreement between them, confirming that the measured relative phases are accurate.

To demonstrate the calibration, the relative phases were all tuned to be zero using the RF-PSs. Figure 6 shows the pulses that were formed when the slave lasers were all in phase with one another. There is good agreement between the measured and expected shape of the waveform.

B. Sinc-Spectrum Rectangular Pulses

A rectangular pulse train with a repetition rate of 100 GHz and a duty cycle of 50% was targeted using the sinc-shaped spectrum illustrated in Fig. 2. The targeted relative powers of the slave lasers were the square of the electric field amplitudes, and the relative phases of the positive amplitude components were set to zero, while the negative components were set to π. Rectangular pulses are ideal as a gating signal for all-optical switching using the nonlinear Kerr effect. The constant power across the pulse can help reduce distortions (e.g., pulse breakup) of switched pulses [30] and has been demonstrated to improve timing jitter tolerance in optical time division multiplexing systems [31].

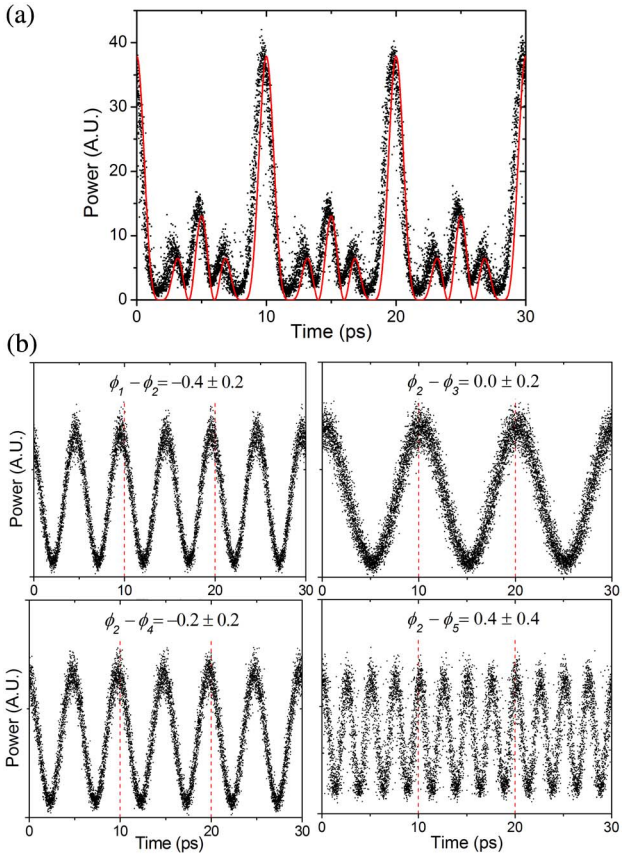

Fig. 6. (a) 100 GHz pulses formed by aligning the phases of the slave lasers (dots, measured; red line, calculated). (b) Measured relative phases of the slave lasers when set to zero using the calibration data.

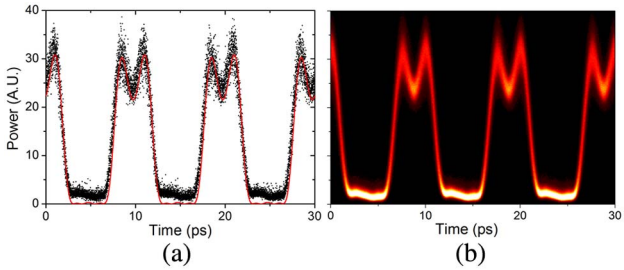

Fig. 7. (a) Measured (black) and targeted (red) waveforms using a sinc-shaped spectrum. (b) Heat map of a 2 min persistence measurement showing the frequency of the measured samples.

The measured waveform is shown in Fig. 7(a), and the measured and targeted relative powers and phases of the slave lasers are given in Table 2. Figure 7(a) shows good agreement between the measured and targeted waveforms despite the slight mismatch between the measured and targeted relative phases. With only five nonzero components, significant deviation from ideal flat-top rectangular pulses is predicted, as can be seen in the targeted waveform.

The measured waveform does not decrease all the way to zero between pulses. This was due to the OSO having a small measurement offset, which was likely due to internal noise and the limited bandwidth. This offset may also have been partly due to the polarizations of the slave lasers not being perfectly aligned.

The stability of the waveform was characterized by continuously measuring the waveform on the OSO for 2 min. This data is shown in Fig. 7(b) as a heat map, which shows the frequency of the measured samples, with black representing zero frequency and white representing the maximum frequency of the samples. The heat map was well defined, which shows that the waveform was stable over the measurement time. The shape of the waveform remained stable for over an hour, which was significantly longer than the heat map measurement time.

C. Apodization—Flat Top

The limited number of frequency components available resulted in a large ripple across the top of the sinc-spectrum rectangular pulses. Apodization of the sinc-shaped spectrum was employed to smooth this ripple at the cost of reducing the sharpness at the edges of the pulses. This was done by attenuating the ± 100 and ± 300 GHz components of the sinc-spectrum by approximately 1 and 7 dB, respectively.

Table 2. Slave Lasers for Sinc-Shaped Spectrum

	Relative Power (dB)		Relative Phase (rad)	
Laser Index	Targeted	Measured	Targeted	Measured
1	−13.5	−12.8	π	3.6 ± 0.2
2	−3.9	−3.9	NA	NA
3	0	0	0	0.1 ± 0.2
4	−3.9	−4.2	0	0.3 ± 0.2
5	−13.5	−13.1	π	3.6 ± 0.4

Table 3. Slave Lasers for Apodized Sinc-Shaped Spectrum

	Relative Power (dB)		Relative Phase (rad)	
Laser Index	Targeted	Measured	Targeted	Measured
1	−20.0	−19.9	π	2.8 ± 0.2
2	−5.0	−4.9	NA	NA
3	0	0	0	-0.1 ± 0.2
4	−5.0	−4.9	0	-0.2 ± 0.2
5	−20.0	−20.0	π	2.7 ± 0.4

The targeted and measured powers and phases are given in Table 3.

The measured waveform is shown in Fig. 8(a). Again, there is good agreement between the measured and expected waveform. The apodization had the desired effect of significantly smoothing the top of the pulses. The pulses exhibited the same level of stability as the pulses generated using the sinc-shaped spectrum as shown in the heat map in Fig. 8(b).

D. Dark-Parabolic Pulses

Waveforms with a sinc^2 spectrum were also targeted. These waveforms have a linearly increasing and decreasing (triangular) electric field shape, which corresponds to pulses with a parabolic power profile in between them. These are commonly referred to as dark-parabolic pulses, in contrast to similaritons, which are also known as bright-parabolic pulses. Similar to bright-parabolic pulses, dark versions can be utilized in cross-phase modulation (XPM) experiments to impart a linear chirp onto a signal. This feature has previously been used to perform optical Fourier transforms and to eliminate linear distortions in signals [32].

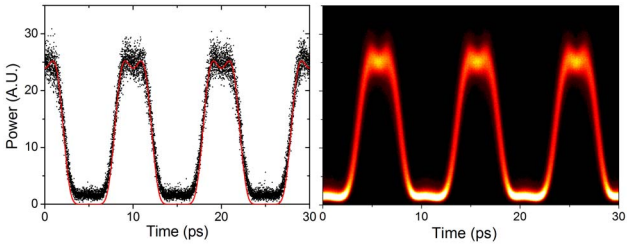

Fig. 8. (a) Measured (black) and targeted (red) waveforms using an apodized sinc-shaped spectrum. (b) Heat map of a 2 min persistence measurement.

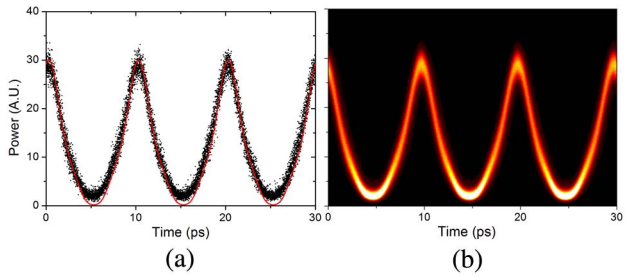

Fig. 9. (a) Measured (black) and targeted (red) waveforms using a sinc^2-shaped spectrum. (b) Heat map of a 2 min persistence measurement.

Table 4. Slave Lasers for Sinc^2-Shaped Spectrum

	Relative Power (dB)		Relative Phase (rad)	
Laser Index	Targeted	Measured	Targeted	Measured
1	−27.0	−27.4	0	0.0 ± 0.1
2	−7.8	−8.3	NA	NA
3	0	0	0	-0.1 ± 0.2
4	−7.8	−8.3	0	-0.2 ± 0.2
5	−27.0	−28.0	0	-0.3 ± 0.4

The targeted and measured relative powers and phases are given in Table 4. As compared to the sinc-spectrum waveforms, the targeted relative powers were squared, and the relative phases became equal. The measured waveform and 2 min heat map are shown in Fig. 9. Similar to the previous waveforms, these show good agreement between the measured and targeted waveforms, and a high level of stability.

5. DEMONSTRATION OF PHASE CONTROL: DISPERSION COMPENSATION

Dispersion compensation was performed to demonstrate a similar functionality of the synthesized waveforms as compared to a programmable phase filter. Apodized sinc-spectrum waveforms were generated, as demonstrated earlier (Fig. 8) and shown in Fig. 10(a), and propagated through 2 km of standard single-mode fiber (SMF-28). The chromatic dispersion of 2 km of fiber was sufficient to significantly distort the waveform, as shown in Fig. 10(b).

The waveforms were reformed to the desired shape at the output of the length of fiber by introducing the opposite dispersion into the input waveform, thus precompensating for the fiber dispersion. This was accomplished by adjusting the relative phases between the lasers using the RF-PSs. Figures 10(c) and 10(d) show the dispersion precompensated waveforms at the input and output of the 2 km fiber, respectively. As expected, the dispersion precompensated output [Fig. 10(d)] is a good reproduction of the original input

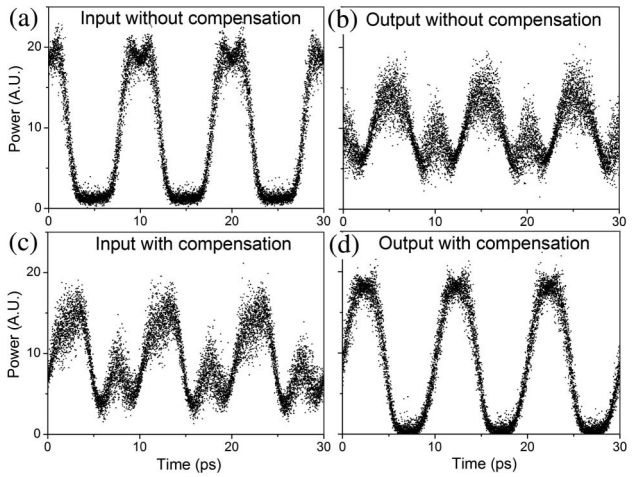

Fig. 10. Flat-top (apodized sinc-spectrum) waveforms at (a) input and (b) output of a 2 km length of single-mode optical fiber without any dispersion compensation. The waveforms after dispersion precompensation at the input and output are shown in (c) and (d), respectively.

[Fig. 10(a)]. The waveforms in Figs. 10(b) and 10(c) also resemble one another due to the symmetry of the system.

6. CONCLUSION

We have shown how to address various challenges to realize Fourier synthesis of high-repetition-rate waveforms. In contrast to existing pulse shaping techniques, Fourier synthesis allows for easily tunable repetition rates. High-power and highly stable waveforms can also be generated with high SNR by using a larger number of lasers and operating at higher powers. The approach is not limited to any wavelength, as no amplifiers are needed.

In our demonstration we used five semiconductor lasers, which were phase locked to a common optical frequency comb. Active stabilization of the relative optical path lengths between the lasers was utilized to overcome thermal fluctuations and drift and allow for the control of the relative phases between the lasers as they were combined. Independent control of the relative phase and powers of the lasers allowed pulse trains with various optical power (e.g., rectangular and dark parabolic) and phase profiles to be generated with high stability. As an example, we demonstrated control of the phase profile to precompensate for the chromatic dispersion acquired by generated pulses propagating though 2 km of standard optical fiber.

The complexity of the waveforms demonstrated was limited by the number of lasers used for the Fourier synthesis. However, our experiments demonstrate the feasibility and stability of the approach. The technique would become particularly interesting if the many lasers required could be integrated on to the same photonic chip. We believe this photonic integration could potentially lead to a compact, portable, stable, and practical optical waveform synthesizer suitable for a diverse range of scientific and engineering applications.

FUNDING INFORMATION

Engineering and Physical Sciences Research Council (EPSRC) (EP/I01196X/1, EP/K003038/1).

ACKNOWLEDGMENT

The authors thank Dr. Francesca Parmigiani for helpful discussions relating to this work.

REFERENCES

1. R. P. Scott, N. K. Fontaine, J. P. Heritage, and S. J. B. Yoo, "Dynamic optical arbitrary waveform generation and measurement," Opt. Express **18**, 18655–18670 (2010).
2. D. J. Geisler, N. K. Fontaine, R. P. Scott, T. He, L. Paraschis, O. Gerstel, J. P. Heritage, and S. J. B. Yoo, "Bandwidth scalable, coherent transmitter based on the parallel synthesis of multiple spectral slices using optical arbitrary waveform generation," Opt. Express **19**, 8242–8253 (2011).
3. F. Parmigiani, P. Petropoulos, M. Ibsen, and D. J. Richardson, "Pulse retiming based on XPM using parabolic pulses formed in a fiber Bragg grating," IEEE Photon. Technol. Lett. **18**, 829–831 (2006).
4. F. Parmigiani, M. Ibsen, T. T. Ng, L. Provost, P. Petropoulos, and D. J. Richardson, "An efficient wavelength converter exploiting a grating-based saw-tooth pulse shaper," IEEE Photon. Technol. Lett. **20**, 1461–1463 (2008).
5. C. Mendonça, U. Neves, I. Guedes, S. Zilio, and L. Misoguti, "Coherent control of optically induced birefringence in azoaromatic molecules," Phys. Rev. A **74**, 025401 (2006).
6. T. Laarmann, I. Shchatsinin, P. Singh, N. Zhavoronkov, C. P. Schulz, and I. Volker Hertel, "Femtosecond pulse shaping as analytic tool in mass spectrometry of complex polyatomic systems," J. Phys. B **41**, 074005 (2008).
7. N. Dudovich, D. Oron, and Y. Silberberg, "Single-pulse coherently controlled nonlinear Raman spectroscopy and microscopy," Nature **418**, 512–514 (2002).
8. D. Geisler, N. Fontaine, T. He, R. P. Scott, L. Paraschis, J. P. Heritage, and S. J. B. Yoo, "Modulation-format agile, reconfigurable Tb/s transmitter based on optical arbitrary waveform generation," Opt. Express **17**, 15911–15925 (2009).
9. A. M. Weiner, "Femtosecond pulse shaping using spatial light modulators," Rev. Sci. Instrum. **71**, 1929–1960 (2000).
10. S. T. Cundiff and A. M. Weiner, "Optical arbitrary waveform generation," Nat. Photonics **4**, 760–766 (2010).
11. A. M. Weiner, "Ultrafast optical pulse shaping: a tutorial review," Opt. Commun. **284**, 3669–3692 (2011).
12. J. W. Wilson, P. Schlup, and R. A. Bartels, "Ultrafast phase and amplitude pulse shaping with a single, one-dimensional, high-resolution phase mask," Opt. Express **15**, 8979–8987 (2007).
13. J. Pleumeekers, E. Strzelecka, K. Yap, A. James, P. Studenkov, P. Debackere, T. Nguyen, S. Agashe, N. Kim, V. Lal, J. Won, C. Hill, Z. Wang, I. Dudley, A. Dentai, Q. Chen, D. Christini, R. Salvatore, D. Lambert, M. Lai, M. Missey, R. Muthiah, J. Rossi, P. Liu, S. Craig, R. Schneider, M. Reffle, and F. Kish, "Manufacturing progress for InP-based 500 Gb/s photonic integrated circuits," in *CS MANTECH Conference* (CS ManTech, 2013), pp. 19–22.
14. C. Hayes and L. Laughman, "Generation of coherent optical pulses," Appl. Opt. **16**, 263–264 (1977).
15. M. Hyodo, N. Onodera, and K. S. Abedin, "Fourier synthesis of 257 GHz optical pulse train by phaselocking of three continuous-wave semiconductor lasers," Electron. Lett. **35**, 564–566 (1999).
16. M. Hyodo, K. Abedin, and N. Onodera, "Generation of arbitrary optical waveforms by Fourier synthesis using three continuous-wave semiconductor lasers," Electron. Lett. **36**, 224–225 (2000).
17. M. Hyodo, K. S. Abedin, and N. Onodera, "Fourier synthesis of 1.8-THz optical-pulse trains by phase locking of three independent semiconductor lasers.," Opt. Lett. **26**, 340–342 (2001).
18. L. R. Brothers, D. Lee, and N. C. Wong, "Terahertz optical frequency comb generation and phase locking of an optical parametric oscillator at 665 GHz," Opt. Lett. **19**, 245–247 (1994).
19. A. E. Siegman, *Lasers* (University Science Books, 1986).
20. F. Mogensen, H. Olesen, and G. Jacobsen, "Locking conditions and stability properties for a semiconductor laser with external light injection," IEEE J. Quantum Electron. **21**, 784–793 (1985).
21. C. Walton, A. C. Bordonalli, and A. J. Seeds, "High-performance heterodyne optical injection phase-lock loop using wide linewidth semiconductor lasers," IEEE Photon. Technol. Lett. **10**, 427–429 (1998).
22. A. C. Bordonalli, C. Walton, and A. J. Seeds, "High-performance phase locking of wide linewidth semiconductor lasers by combined use of optical injection locking and optical phase-lock loop," J. Lightwave Technol. **17**, 328–342 (1999).
23. Y. J. Kim, Y. Kim, B. J. Chun, S. Hyun, and S. W. Kim, "All-fiber-based optical frequency generation from an Er-doped fiber femtosecond laser," Opt. Express **17**, 10939–10945 (2009).
24. D. S. Wu, R. Slavík, G. Marra, and D. J. Richardson, "Direct selection and amplification of individual narrowly spaced optical comb modes via injection locking: design and characterization," J. Lightwave Technol. **31**, 2287–2295 (2013).
25. D. S. Wu, D. J. Richardson, and R. Slavík, "Selective amplification of frequency comb modes via optical injection locking of a semiconductor laser: influence of adjacent unlocked comb modes," Proc. SPIE **8781**, 87810J (2013).

26. B. Kelly, R. Phelan, D. Jones, C. Herbert, J. O'Carroll, M. Rensing, J. Wendelboe, C. B. Watts, A. Kaszubowska-Anandarajah, P. Perry, C. Guignard, L. P. Barry, and J. O'Gorman, "Discrete mode laser diodes with very narrow linewidth emission," Electron. Lett. **43**, 1282–1284 (2007).
27. A. Albores-Mejia, H. Kuwatsuka, H. Shoji, and H. Ishikawa, "Full-band injection-locking properties of a monolithically integrated tunable laser with single stripe structure," in *European Conference and Exhibition on Optical Communication* (Optical Society of America, 2012), P2.13.
28. L. Liu, Z. Tong, A. Wiberg, B. Kuo, E. Myslivets, N. Alic, and S. Radic, "Digital multi-channel stabilization of four-mode phase-sensitive parametric multicasting," Opt. Express **22**, 18379–18388 (2014).
29. Y. Ma, P. Zhou, X. Wang, H. Ma, X. Xu, L. Si, Z. Liu, and Y. Zhao, "Coherent beam combination with single frequency dithering technique," Opt. Lett. **35**, 1308–1310 (2010).
30. A. Weiner, Y. Silberberg, H. Fouckhardt, D. E. Leaird, M. A. Saifi, M. J. Andrejco, and P. W. Smith, "Use of femtosecond square pulses to avoid pulse breakup in all-optical switching," IEEE J. Quantum Electron. **25**, 2648–2655 (1989).
31. J. Lee, L. Oxenløwe, and M. Ibsen, "All-optical TDM data demultiplexing at 80 Gb/s with significant timing jitter tolerance using a fiber Bragg grating based rectangular pulse switching technology," J. Lightwave Technol. **21**, 2518–2523 (2003).
32. T. Hirooka and M. Nakazawa, "Fourier transformation using XPM with a dark parabolic pulse," IEEE Photon. Technol. Lett. **20**, 1869–1871 (2008).